X-Ray Analysis of the Structure of Premelted Layers at Ice Interfaces

2000 Jpn. J. Appl. Phys. 39 6696

(http://iopscience.iop.org/1347-4065/39/12R/6696)

Jpn. J. Appl. Phys. Vol. 39 (2000) pp. 6696–6699
Part 1, No. 12A, December 2000

X-Ray Analysis of the Structure of Premelted Layers at Ice Interfaces

Minoru MARUYAMA, Tomoki SATOI, Shinji TANIGUCHI, Maiko KAWAMURA, Shiro KODERA, Yuko KISHIMOTO and Yoshinori FURUKAWA[1]

Department of Physics, Osaka City University, Osaka 558-8585, Japan
[1]*Institute of Low Temperature Science, Hokkaido University, Sapporo 060-0819, Japan*

(Received June 15, 2000; accepted for publication September 6, 2000)

X-ray diffraction patterns of a premelted layer of ice and liquid water were obtained by a glancing-incidence method. Diffuse intensity patterns due to the premelted layer exhibited variation with temperature. Fourier transformation of the intensity curves gave pair-correlation functions, where the first, second and third peaks were observed in the premelted layer and liquid water. This suggests that there is a short range order in their molecular distribution. The average intermolecular distances between the nearest neighbors were 1–2% smaller in the premelted layer than in liquid water.

KEYWORDS: premelting, surface melting, ice, glancing-angle X-ray diffraction, pair-correlation function, radial distribution function

1. Introduction

Surface melting of ice has been attracting many researchers since Faraday's original work.[1)] Various recent studies have demonstrated that ice begins to melt from the free surface well below 0°C; the surface premelted layer thickens with increasing temperature and diverges at the transition point to become liquid water.[2,3)] Premelting also occurs at ice/substrate interfaces and at boundaries between ice grains.[2)] It can be enhanced significantly by curvature[2)] and impurity[4)] effects. The thin premelted layer often shows physical properties different from water; for example, its diffusion coefficient[5,6)] and refractive index[7)] are intermediate between the values for ice and those for water. Thus it is often called a quasi-liquid layer. Molecular dynamics simulations reveal a similar picture on a molecular scale.[8)] Premelting is not unique to ice, but is common to most solids.[9)] It is regarded as a universal phenomenon that takes place as a result of the reduction in interfacial free energy caused by the formation of a liquid-like layer close to the melting point.

Numerous experimental techniques have been employed to characterize the premelted layer at solid interfaces.[9)] Ice has large vapor pressure near the melting point, so that conventional tools for vacuum use are inappropriate to this study. X-ray scattering as well as neutron scattering is best suited to investigate the structure of ice and water. Glancing-angle X-ray diffraction[10)] is a powerful tool in the study of thin films and interfaces. In particular, below the critical angle for total external reflection, it is possible to probe the uppermost layers by specular reflection. Using this technique, Lied *et al.*[11)] showed that the surface melted layer logarithmically grows in thickness with temperature, by observing the decay of solid signals (Bragg scattering intensities). Another approach to investigate disordered materials is to measure directly the scattering signal from the liquid and obtain the pair-correlation function that gives the average distribution of neighboring molecules. This type of X-ray diffraction in liquid water[12,13)] demonstrated that water has a short range order: an H_2O molecule has approximately 4.4 nearest-neighbor molecules at a distance of 2.90 Å at room temperature. By using glancing-angle X-ray diffraction, Kouchi *et al.*[14)] observed a liquid-like diffuse pattern scattered from the surface of ice. We extend and improve this qualitative work and report here a quantitative analysis of intensity curves, whose Fourier transformation gives a spatial distribution of H_2O molecules within the premelted layer at ice interfaces.

2. Experiment

Diffraction measurements were carried out using a diffractometer specially designed for the study of thin films and surfaces. Most of these studies have been performed using strong X-ray sources, such as a rotating anode or synchrotron. As a source, we used a standard laboratory X-ray tube, which yielded sufficient intensity scattered from the surface of water or ice. The sample surface always remained horizontal so that the water surface could also be studied using the diffractometer.

Figure 1 shows a schematic of an ice sample and its surroundings in the diffractometer. An X-ray beam, which was emitted from an X-ray tube with a Mo target and collimated by Soller slits, was incident on the ice at a glancing angle. The angle was chosen at 1° to observe the surface region of the ice. The incident beam had a line cross section (0.2 mm × 10 mm) at the sample position. The X-ray beams scattered by the sample were collimated to 3 mm by slits and then monochromated by reflection from flat graphite (0002) planes. The selected wavelength was $\lambda = 0.711$ Å (MoKα radiation). The final intensity was then measured using a scintillation counter as a function of scattering angle 2θ in the range of 4–77°.

Two different samples, a powder sample and a grain sample, were used and are shown in Fig. 2. The powder sample

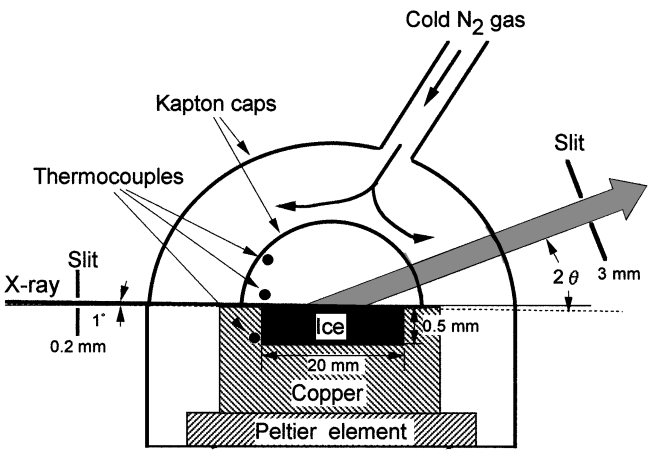

Fig. 1. Sample holder and glancing-angle scattering geometry.

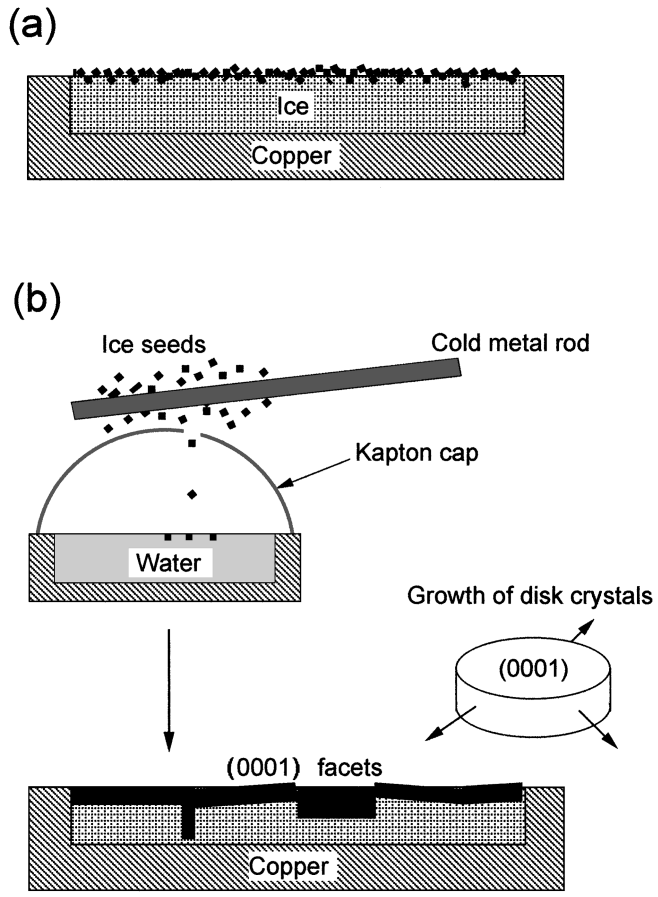

Fig. 2. Sample and preparation. (a) The powder was deposited on a cold ice substrate directly from air moisture. (b) The grains with horizontally oriented (0001) surfaces were grown on water from several disk crystals produced by seeding.

is used to observe grain boundary melting and surface melting, whereas the grain sample with (0001) surfaces is used to observe (0001) surface melting. We prepared these samples directly on a sample holder in the diffractometer as follows. Distilled water was introduced horizontally to a hole ($20\times20\times0.5\,\mathrm{mm}^3$ in volume) made on a copper substrate. To obtain powder samples, the water was frozen spontaneously at about -10°C by cooling the substrate thermoelectrically with Peltier elements attached below it. The resulting ice was cooled to -30°C and then exposed to ambient air for about 30 min to condense water vapor and uniformly form powder on it. After fine powder was obtained, the sample was covered with air-tight Kapton caps to prevent evaporation and to accurately control the sample temperature, as shown in Fig. 1. The transparent Kapton sheets also serve as X-ray windows. The size of ice grains was estimated to be approximately 50 μm. On the other hand, for obtaining horizontally oriented (0001) surface samples, we carried out seeding by placing in air a cold metal rod cooled to the temperature of liquid nitrogen. Air moisture was frozen spontaneously to produce ice crystallites. A number of crystallites fell to the water surface maintained at -0.1°C through a small hole in a Kapton cap and then grew in the shape of a circular disk[15,16] covering the surface. As a result, the sample consists of several grains with nearly horizontal (0001) surfaces.

A series of X-ray runs increasing temperature was performed for an identical sample and then repeated for different samples. One run at a specified temperature took 20 min for the 2θ scan. Near 0°C, the temperature was carefully increased gradually at intervals of 0.01–0.04°C, because the premelted layer grew abruptly. It was, therefore, necessary to control temperature very accurately near 0°C. For this reason, two Kapton caps were placed over the sample: the flow of cold nitrogen gas was sent to an open space between the two caps to maintain the sample at a constant and uniform temperature, in addition to the thermoelectric cooling from the bottom. The temperatures were measured with three CRC thermocouples: one was in the substrate, and the others were above the sample surface. The three agreed in their measurements within 0.1°C.

3. Results and Discussion

3.1 Diffraction pattern

Figure 3 shows the variation in diffraction patterns with increasing temperature for the powder and (0001) surface samples. The intensity is expressed in arbitrary units. The temperatures indicated are those of the substrate. The two samples yielded sharp peaks due to crystalline ice at low temperatures. The difference in crystallinity gave different appearances of the peaks. As temperature increased, diffuse patterns grew with an asymmetrically broadened peak. These patterns are

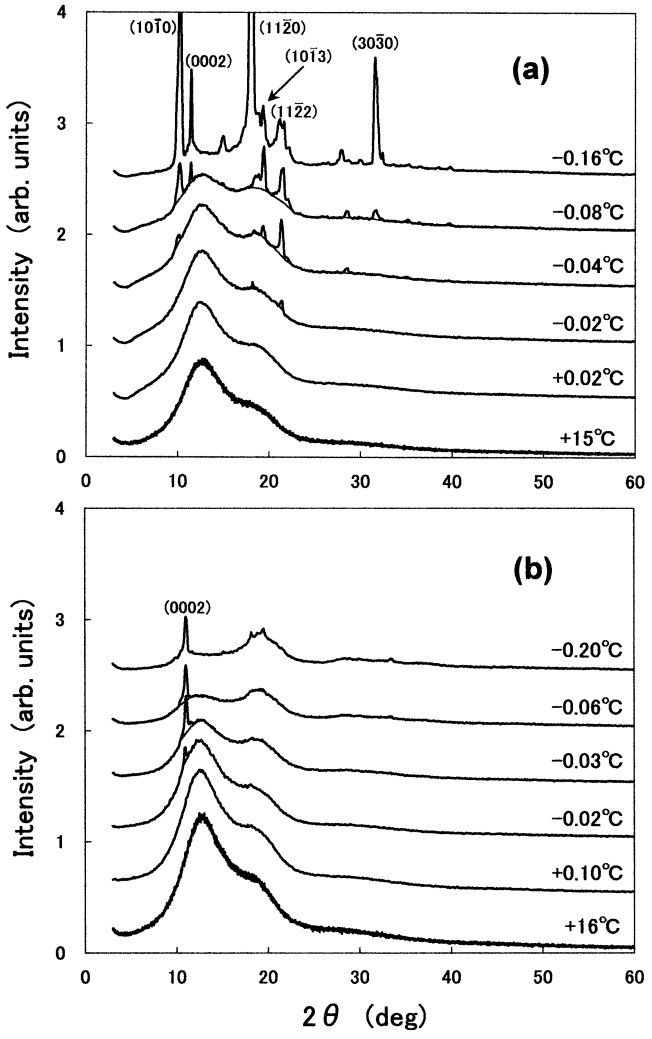

Fig. 3. Observed intensity curves as a function of scattering angle 2θ; (a) powder and (b) (0001) surfaces. Peak intensities due to ice contributions were cut and smooth curves are shown for the premelted layer.

due to the premelt liquid exhibiting similar shapes and variations in temperature in the two samples. Hereafter, we describe the patterns of the powder sample. At −0.16°C, Bragg reflections expected from the hexagonal structure of ice are all visible. The peak heights remain unchanged from −20°C to −0.1°C. Close to 0°C, the patterns change abruptly: at −0.08°C the peaks become small; at −0.04°C and −0.02°C some peaks disappear in the diffuse pattern, which instead grows asymmetrically; no peaks were observed at +0.02°C. The diffuse patterns are typical for disordered materials such as liquids and amorphous solids,[17,18] and are in good agreement with those of liquid water.[12,19] Morgan and Warren[12] observed that the asymmetry in the broad peak decreases with temperature and disappears above 83°C. This was interpreted as a result of the increase in intermolecular distance with increasing temperature based on analyzing radial distribution curves. Our obtained diffuse patterns below 0°C are similar to that of water above 0°C. We attribute these patterns to increasing premelt liquid, which coexists with shrinking core ice. The ice peaks are cut and thereby the diffuse components are available, as shown in Fig. 3. These intensity curves are used for data reduction for the premelted layer. The variation in diffuse patterns with temperature suggests that there is a gradual change in the structure of the premelted layer. Fourier transformed correlation functions, described below, provide the quantitative information about the structure of the premelted layer.

3.2 Pair-correlation function

According to conventional data reduction,[17,19] a few corrections were done for measured intensity (raw data), as shown in Fig. 3. The effects of polarization and absorption by X-ray scattering were first corrected, and the resulting intensity was normalized and expressed in electron units per molecule; finally, subtracting an incoherent component (Compton scattering), we obtained the intensity $I(s)$ as a function of the scattering vector $s(\theta) = (4\pi/\lambda)\sin\theta$.

The intensity $I(s)$ represents the component scattered coherently by a molecule in a liquid phase. In an H_2O molecule, eight electrons have spherical orbitals around the oxygen nucleus, whereas two in the hydrogens are in off-center orbitals; the overall electron distribution is nearly spherical. Assuming that an H_2O molecule has a spherical distribution of electron density like that of an argon atom, we can derive the simple expression:[13]

$$I(s) = \langle F(s)^2\rangle + \langle F(s)^2\rangle \int_0^\infty 4\pi r^2[\rho(r) - \rho_0]\frac{\sin(sr)}{sr}\,dr. \tag{1}$$

The first term $\langle F(s)^2\rangle$ represents the intramolecular scattering intensity due to an isolated H_2O molecule with random orientations, and can be calculated based on its geometry and atomic scattering intensity data of H and O atoms. The brackets $\langle\ \rangle$ denote the average over all molecular orientations. The second term is important; it represents the intermolecular scattering intensity due to randomly distributed molecules in the liquid, related to the H_2O–H_2O pair-correlation function. The term $\rho(r)$ is the local molecular density expressed in molecules/Å^3 at a distance r from the center of any molecule. The term ρ_0 is the uniform, bulk-water density corresponding to the mass density of 1 g/cm^3 and is 0.0334 molecules/Å^3.

The reduced intensity $i(s)$, the integral in eq. (1), is extracted as

$$i(s) = \frac{I(s) - \langle F(s)^2\rangle}{\langle F(s)^2\rangle}, \tag{2}$$

and then

$$si(s) = \int_0^\infty 4\pi r[\rho(r) - \rho_0]\sin(sr)\,dr. \tag{3}$$

Fourier transformation of $si(s)$ yields a radial distribution function $4\pi r^2\rho(r)$ and pair-correlation function $\rho(r)/\rho_0$,

$$4\pi r^2\rho(r) = 4\pi r^2\rho_0 + \frac{2r}{\pi}\int_0^\infty si(s)\sin(sr)\,ds, \tag{4}$$

$$\rho(r)/\rho_0 = 1 + \frac{1}{2\pi^2\rho_0 r}\int_0^\infty si(s)\sin(sr)\,ds. \tag{5}$$

Figures 4(a) and 4(b) are the pair-correlation functions obtained by the procedure described above, for the intensity curves shown in Figs. 3(a) and 3(b), respectively. The functions give the average distribution of neighboring molecules as a function of distance r from any molecule. The first peak represents the nearest neighbors, and the peak position gives the average distance of separation. For reference, Fig. 4 presents the corresponding positions in ice that has a regular molecular distribution, consisting of a local tetrahedral bond-

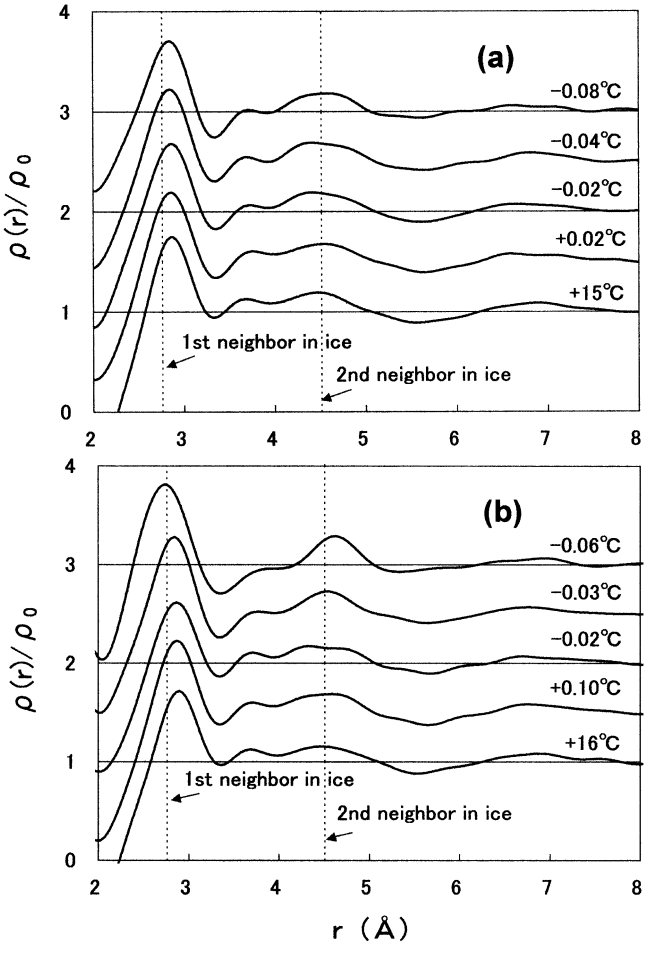

Fig. 4. Pair-correlation functions $\rho(r)/\rho_0$ as a function of distance r; (a) powder and (b) (0001) surfaces. The curves for the samples were obtained by Fourier transformation of the intensity curves shown in Figs. 3(a) and 3(b), respectively.

ing and a global hexagonal lattice. The resulting functions increase rapidly with first peaks at $r = 2.76$–2.88 Å and oscillate with decreasing amplitude around the asymptotic value of unity. There are also second peaks around 4.5 Å and third peaks around 7 Å. However, these peaks are too small and broad to determine accurately their distances of separation. Beyond 8 Å, $\rho(r)/\rho_0 \approx 1$, representing a uniform molecular distribution at such large distances. These findings show that there remains a short range order in the premelted layer and liquid water.

In Fig. 5, the nearest-neighbor distance (i.e., the nearest neighboring oxygen-oxygen distance) is plotted as a function of temperature. The accuracy is approximately 0.01 Å based on the peak positions. Ice and water levels are also shown in the figure. For water at 4°C and supercooled water at −3°C, we also measured the diffraction intensity curves and obtained a value as 2.87 Å. The distance in the premelted layer is slightly smaller than that in water and larger than that in ice. The difference in distance between the premelted layer and water is 1–2%, but is still significant. Immediately above 0°C, the distance becomes equal to that of water. We also determined the number of first nearest-neighbors or the coordination number by integrating the first peak area in the radial distribution functions obtained using eq. (4): $\int 4\pi r^2 \rho(r) dr$. The estimates gave values of 4.2 to 4.5 for the premelted layer and also for liquid water; however there is no discernible difference between them. These results are relevant to the length scale of a surface region we observed using X-ray beams. We roughly estimate that X-rays of 0.711 Å wavelength penetrate into ice nearly 0.1 mm from the surface at a 1° glancing angle. The scattered intensity provides the structural information averaged over the region. A surface thickness of 0.1 mm is very large and thus our premelt liquid had a thickness well beyond the μm level. This magnitude was probably caused by a rapid growth of the premelted layer immediately below the melting point.[7] For this reason, our premelted layer showed properties similar to those of water.

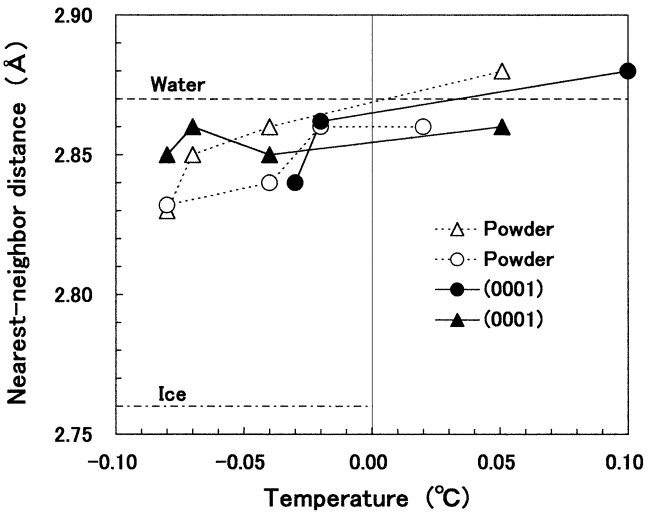

Fig. 5. Nearest-neighbor intermolecular distance in premelted layer, liquid water, and solid ice.

4. Conclusions

We performed a direct observation of a premelted layer at ice interfaces using glancing-angle X-ray diffraction. The scattered intensity patterns were like those of liquid water but were slightly different. Pair-correlation functions, obtained by Fourier analysis, directly provided data on average intermolecular distances in a disordered system without any fitting parameters. The first nearest-neighbor distance ranged from 2.83 Å to 2.86 Å, independent of whether premelting occurred at grain boundaries or (0001) surfaces; for liquid water the value was 2.87 Å. The second and third neighbors were also observed although accurate distances were not obtained. These findings suggest that the premelted layer at ice interfaces still has a short range order, as in liquid water. In this experiment the premelted layer was observed very close to the melting point, i.e., between −0.1°C and 0°C, and probably had a magnitude of thickness in the μm range. Such a large length scale did not result in much difference in intermolecular distance between the premelted layer and liquid water. Future measurements using synchrotron X-rays will reveal the quasi-liquid features more clearly by observing a thinner premelted layer that appears at lower temperatures.

Acknowledgements

We would like to thank A. Kouchi, J. S. Wettlaufer and J. G. Dash for helpful discussions. This work was partially supported by a Grant-in-Aid for Scientific Research No. 09640405 from the Ministry of Education, Science, Sports and Culture, and was carried out under the approval of the Institute of Low Temperature Science, Hokkaido University (proposal no. 99-61)

1) M. Faraday: Philos. Mag. **17** (1859) 162.
2) J. G. Dash, H. Fu and J. S. Wettlaufer: Rep. Prog. Phys. **58** (1995) 115, and references therein.
3) J. S. Wettlaufer and J. G. Dash: Sci. Am. **282** (2000) 50.
4) J. S. Wettlaufer: Phys. Rev. Lett. **82** (1999) 2516.
5) Y. Mizuno and N. Hanafusa: J. Phys. (Paris) **48** (1987) C1-511.
6) M. Maruyama, M. Bienfait, J. G. Dash and G. Coddens: J. Cryst. Growth **118** (1992) 33.
7) Y. Furukawa, M. Yamamoto and T. Kuroda: J. Cryst. Growth **82** (1987) 655.
8) H. Nada and Y. Furukawa: Surf. Sci. **446** (2000) 1.
9) J. G. Dash: Contemp. Phys. **30** (1989) 89.
10) P. S. Pershan: J. Phys. (Paris) **50** (1989) C7-1.
11) A. Lied, H. Dosch and J. H. Bilgram: Phys. Rev. Lett. **72** (1994) 3554.
12) J. Morgan and B. E. Warren: J. Chem. Phys. **6** (1938) 666.
13) A. H. Narten and H. A. Levy: J. Chem. Phys. **55** (1971) 2263.
14) A. Kouchi, Y. Furukawa and T. Kuroda: J. Phys. (Paris) **48** (1987) C1-675.
15) K. Arakawa and K. Higuchi: J. Fac. Sci., Hokkaido Univ., Ser. II, **4** (1952) 201.
16) K. Arakawa: J. Glaciol. **2** (1955) 463.
17) B. E. Warren: *X-Ray Diffraction* (Addison-Wesley, Reading, Massachusetts, 1969) p. 116.
18) Y. Kobashi and S. Kodera: Jpn. J. Appl. Phys. **37** (1998) 2590.
19) H. A. Levy, M. D. Danford and A. H. Narten: ORNL Rep. ORNL-3960 (1966).